ISSN NO: 9726-001X
Volume 10 Issue 03 2022

JOURNAL OF CURRENT SCIENCE

SIMULATING MULTISCALE PLASTICITY USING POLYPROPYLENE SPHERULITE STRUCTURE

Dr.Pratap.S.Kulkarni,Dr.B.H.Manjunath,Dr.Naveen.R

Asst. Prof,Prof. & HOD,Asst. Prof

spratapkulkarni@gmail.com, bhmanj@gmail.com, shivaganesh.ng@gmail.com

Department of Mech, Proudhadevaraya Institute of Technology, Abheraj Baldota Rd, Indiranagar, Hosapete, Karnataka-583225

Abstract
Both amorphous and crystalline polymers fall into the larger category of polymeric materials. The exceptional formability and low weight of polypropylene (PP) make it an ideal material for a broad variety of applications, from commonplace items to machine components. Crystalline polymers, such as PP, exhibit the following multiscale structures. Spherulites are formed as a result of the radial growth of lamellae that include both amorphous and crystalline phases. The moulding conditions dictate the size and crystallinity of the spherulites that are filled with PP. The deformation of polymeric crystalline materials has been the subject of much investigation. A lot is still out in the air, however, and that includes how multiscale structures affect the crystalline polymer's material and mechanical characteristics. In materials research and engineering, it is desirable to have a computer model that can replicate PP's characteristics using multiscale structures. This work investigates the impact of the amorphous and crystalline phases of polypropylene (PP) on macroscopic stress-strain behaviour via the use of a polymer plasticity simulation that takes into account a spherulite structure. By adjusting the cooling conditions, PP samples with varying crystallinity may be produced. A computer model is fed data on specimen crystallinity derived from experimental findings. Our investigation into how spherulite structures impact the material characteristics of PP is comprehensive.

Key words: High polymer materials, Finite element method, Amorphous, Law of mixture, Constitutive equation, Stress-strain measurement, Plasticity, Spherulite, Polypropylene

1. Introduction

Polymeric materials are divided broadly into two categories: amorphous and crystalline polymers. Polypropylene (PP) is widely used from daily necessities to machine parts because of its high formability and light weight. PP that is classified as a crystalline polymer has the following multiscale structures. Lamellae consisting of amorphous and crystalline phases grow radially and spherulites are generated. PP is filled with these spherulites, whose size and crystallinity are determined by the molding conditions. Many researchers have studied the deformation of crystalline polymeric materials. Various calculations have been performed for glassy polymer (Boyce et al., 1989; Arruda and Boyce, 1993a; Wu and Van der Giessen, 1995), since Boyce et al. (1988) presented a three-dimensional model for the deformation of glassy polymer. In order to predict the deformation of polymer, Tomita and Tanaka (1995) modified the model proposed by Boyce et al. (1988) so as to express nonaffine deformation. Parks and Ahzi (1993) simulated the slip deformation of crystalline phase using a crystal plasticity theory proposed by Peirce et al. (1983) for metal materials. Kubo et al. (1986) calculated the distribution of stress in a spherulite using a model considering bifurcation of the crystalline phase. Nada and Shizawa (2008a, 2008b) proposed a molecular-chain plasticity model considering inelasticity based on the local free volume for glassy polymer. Uchida and Tada (2013) proposed a triple-scale model for semi-crystalline polymer and simulated the behavior of a composite phase consisting of amorphous and crystalline phases. However, many points remain unclear, such as the effects of multiscale structures on the material and

mechanical properties of the crystalline polymer. A computational model reproducing the properties of PP based on multiscale structures is desired in the materials science and engineering fields.

In this study, we perform a polymer plasticity simulation considering a spherulite structure consisting of amorphous and crystalline phases in order to investigate the effects of amorphous and crystalline phases of PP on macroscopic stress-strain behavior. PP samples with different crystallinity are prepared by changing the cooling conditions. Information on the crystallinity of spherulite based on experiment results is introduced into the computational model. We thoroughly investigate the effect of spherulite structures on the material properties of PP.

2. Methods of measuring and PP properties

2.1 Experiment procedures

In this study, 1 mm-thick PP sheets are prepared using a heating press. PP samples are heated to 453 K for five minutes. In order to obtain samples of different structures of spherulites, we apply three types of cooling conditions. PP samples are dipped in water at 276 K or 293 K for cooling, or are left to spontaneously cool after being held at 408 K, a temperature at which spherulites grow, for an hour. We refer to the samples prepared by these processes as samples (i), (ii), and (iii). The size of the spherulites is estimated using a polarization microscope for a flaky sample whose thickness is about 6 μm for sample (i) or 10 μm for samples (ii) and (iii). The mean size of the spherulites $\bar{d_S}$ is determined by length along the major and minor axes of the spherulites. The crystallinity of the samples is measured using X-ray diffraction (XRD). The crystallinity χ_C is obtained from the ratio of the integrated intensity for the diffraction peaks of crystalline phase to the total integrated intensity. The mechanical properties of these samples are measured by tensile tests with a universal testing machine. The shapes of the specimens used in the tensile tests are based on the JIS K 7113 2 specimen. We treat the specimens punched from samples (i), (ii), and (iii) as specimens (i), (ii) and (iii).

2.2 Experiment results

Figure 1 depicts polarizing micrographs for samples (i), (ii), and (iii). We observe no spherulite structure in sample (i) because spherulites did not grow sufficiently due to rapid cooling. The mean size of spherulites for sample (ii) was $\bar{d_S} = 33 \pm 3$ μm and that for sample (iii) was $\bar{d_S} = 99 \pm 11$ μm. The spherulites in sample (iii), which was kept at 408K, grew larger than those in sample (ii). Figure 2 depicts the XRD intensity for each sample. All diffraction peaks in Fig. 2 correspond to those for α-phase of PP (Aboulfaraj et al., 1993). The crystallinity calculated from the integrated intensity of Fig. 2 for sample (i) is $\chi_C = 47 \pm 3\%$, that for sample (ii) is $\chi_C = 56 \pm 5\%$, and that for sample (iii) is $\chi_C = 60 \pm 2\%$. The crystallinity increases with increasing spherulite size. No spherulite is observed in sample (i), but the diffraction peaks exist in the XRD intensity in Fig. 2. We assume that spherulite structures, whose diameters are less than 6μm, cannot be observed in sample (i) because they overlap. Figure 3 plots the nominal stress versus nominal strain of each specimen. Softening after yielding, propagation of necking, and rehardening caused by the orientation of molecular chains are observed for all specimens. The mechanical properties of each sample are presented in Table 1.

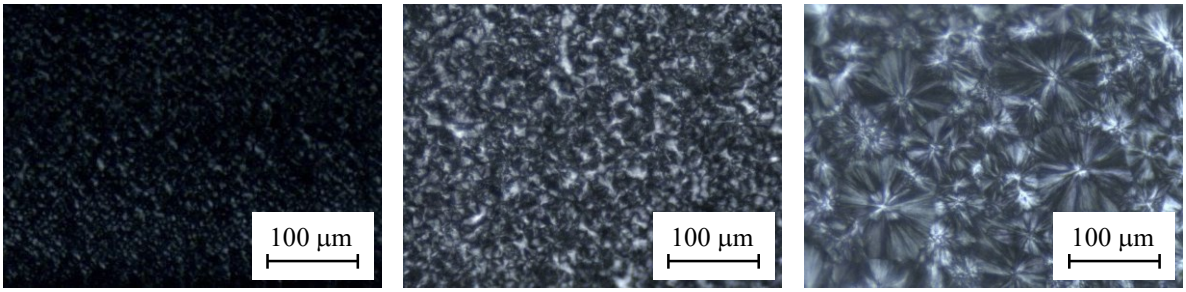

(a) Sample (i) (b) Sample (ii) (c) Sample (iii)

Fig. 1 Polarizing micrograph for the PP samples (i), (ii) and (iii) obtained by the different cooling conditions. Spherulite structure is observed in (b) and (c).

ISSN NO: 9726-001X
Volume 10 Issue 03 2022

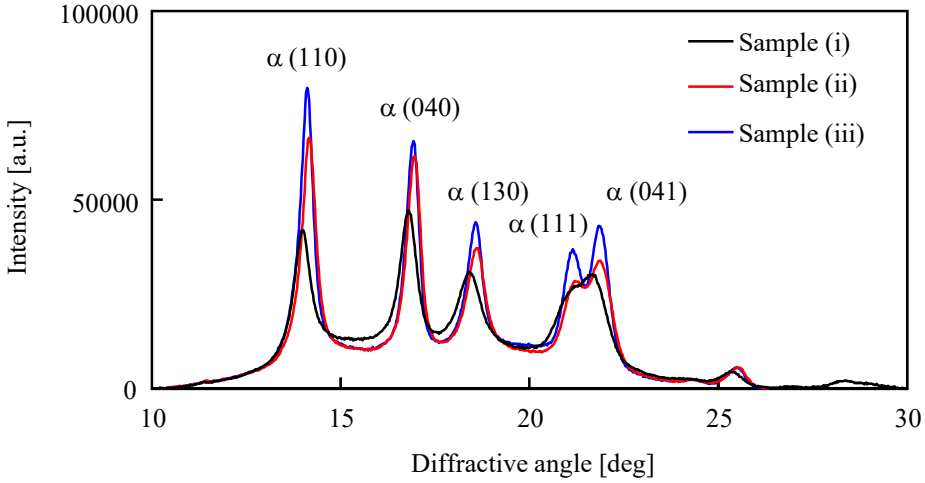

Fig. 2 XRD intensity for PP samples (i), (ii), and (iii). All diffraction peaks correspond to those for α-phase of PP.

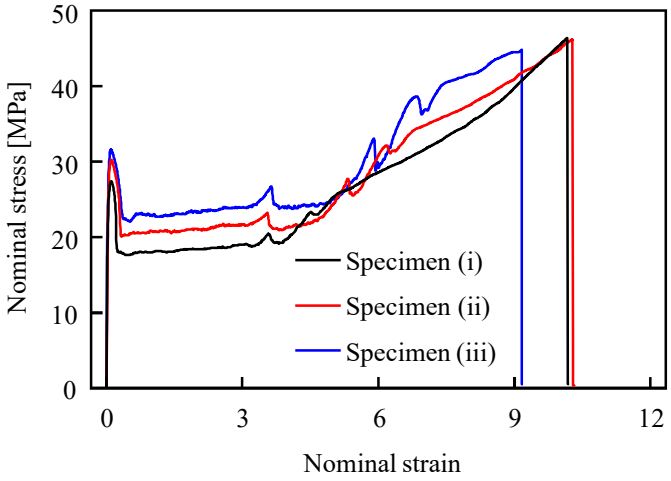

Fig. 3 Nominal stress versus nominal strain curves for specimens (i), (ii), and (iii) obtained by tensile tests.

Table 1 Mechanical properties of samples (i), (ii), and (iii)

Sample	Young's modulus [MPa]	Yield stress [MPa]
(i)	768 ± 23	26.6 ± 0.7
(ii)	842 ± 11	29.7 ± 0.6
(iii)	940 ± 17	31.7 ± 0.5

The yield stress and Young's modulus increase with increasing spherulite size and crystallinity.

3. Multiscale model considering spherulite structure

3.1 Modeling of amorphous phase

In this study, we use molecular-chain network theory (Boyce et al., 1988) to express the deformation of the amorphous phase. Molecular-chain network theory assumes that the amorphous phase has a network structure consisting of a large number of molecular chains. A constitutive equation for the amorphous phase is represented by

ISSN NO: 9726-001X
Volume 10 Issue 03 2022

$$\overset{\circ}{\boldsymbol{T}}_A = \boldsymbol{C}^e_A : \boldsymbol{D}_A - \boldsymbol{C}^e_A : \boldsymbol{D}^p_A = \boldsymbol{C}^e_A : \boldsymbol{D}_A - \boldsymbol{C}^e_A : \left(\frac{\gamma^p}{\sqrt{2}\tau^*} \boldsymbol{T}^{*\prime} \right), \tag{1}$$

where $\overset{\circ}{\boldsymbol{T}}_A$ is the Jaumann rate of Kirchhoff stress for the amorphous phase, $\boldsymbol{C}^e_A$ is the isotropic elastic moduli tensor for the amorphous phase, $\boldsymbol{D}_A$ is the deformation rate tensor for the amorphous phase, $\boldsymbol{D}^p_A$ is the plastic part of $\boldsymbol{D}_A$, $(\boldsymbol{C}^e : \boldsymbol{D})_{ij} \equiv C^e_{ijkl} D_{kl}$, γ^p is the plastic shear strain rate, τ^* is the effective shear stress, and $\boldsymbol{T}^{*\prime}$ is the deviatoric part of the effective stress tensor. The plastic shear strain rate is defined as (Boyce et al., 1988)

$$\gamma^p = \gamma_{0A} \exp\left[-\frac{As}{T} \left\{ 1 - \left(\frac{\tau^*}{s} \right)^{\delta} \right\} \right], \tag{2}$$

where γ_{0A} is the reference shear strain rate, s is the shear strength, T is the absolute temperature, and A is a numerical parameter. The shear strength considering pressure dependency is given by

$$s = s + \alpha p, \tag{3}$$

where s is the athermal shear strength, α is the pressure-dependent coefficient, and p is the pressure given by hydrostatic stress. The evolution equation of the athermal shear strength is represented by

$$\dot{s} = h \left\{ 1 - \frac{s}{s_{ss}} \right\} \dot{\gamma}^p, \tag{4}$$

where h is the hardening ratio and s_{ss} is the saturated shear strength. The effective shear stress and the effective stress tensor are expressed by

$$\tau^* = \sqrt{\frac{1}{2} \boldsymbol{T}^{*\prime} : \boldsymbol{T}^{*\prime}}, \tag{5}$$

$$\boldsymbol{T}^* = \boldsymbol{T}_A - \boldsymbol{B}, \tag{6}$$

where $\boldsymbol{T}_A$ is the Cauchy stress tensor for the amorphous phase and $\boldsymbol{B}$ is the back stress tensor. Principal components of the back stress tensor, which is based on an eight-chain model (Arruda and Boyce, 1993b) is given by

$$b_i = \frac{1}{3} nkT\sqrt{N} \frac{\nu_i^p - \lambda^2}{\lambda} L^{-1}\left(\frac{\lambda}{\sqrt{N}} \right), \tag{7}$$

where b_i represents the principal components of the back stress tensor, n is the number of molecular chains per unit volume, k is the Boltzmann constant, N is the mean number of segments in a molecular chain, ν_i^p is the principal

plastic stretch, $\lambda = \boldsymbol{v}^{p2}/3$, and $L(x) = \coth x - 1/x$ is the Langevin function. When the number of entangled points of molecular chains is constant, the deformation becomes affine. Tomita (2000) proposed a nonaffine eight-chain model expressing the change in the number of entangled points. We use the affine eight-chain model in order to simplify the calculations.

3.2 Modeling of crystalline phase

Since the crystalline phase consists of folded molecular chains in a uniform array, plastic deformation of the crystalline phase is caused by slip deformation on specified planes (Bowden and Young, 1974). In this study, the plastic deformation of the crystalline phase is described by crystal plasticity theory (Peirce et al., 1983). A constitutive equation of the crystal plasticity theory is given by

$$\overset{\nabla}{\boldsymbol{T}}_C = \boldsymbol{C}_C^e : \boldsymbol{D}_C - \boldsymbol{C}_C^e : \boldsymbol{D}_C^p = \boldsymbol{C}_C^e : \boldsymbol{D}_C - \sum_{\alpha} \boldsymbol{C}_C^e : (\boldsymbol{s}^{(\alpha)} \otimes \boldsymbol{m}^{(\alpha)})_S \gamma^{(\alpha)}, \tag{8}$$

where $\overset{\nabla}{\boldsymbol{T}}_C$ is the corotational rate of Cauchy stress for the crystalline phase, $\boldsymbol{C}_C^e$ is the isotropic elastic moduli tensor for the crystalline phase, $\boldsymbol{D}_C$ is the deformation rate tensor for the crystalline phase, $\boldsymbol{D}_C^p$ is the plastic part of $\boldsymbol{D}_C$, $(\boldsymbol{s}^{(\alpha)} \otimes \boldsymbol{m}^{(\alpha)})_S$ is the Schmid tensor, $\boldsymbol{s}^{(\alpha)}$ is the slip direction of slip system α, $\boldsymbol{m}^{(\alpha)}$ is the normal direction of the slip plane, and $\gamma^{(\alpha)}$ is the slip rate. The slip rate is determined by the slip-rate hardening law by Pan and Rice (1983).

$$\gamma^{(\alpha)} = \gamma_{0C} \frac{\tau^{(\alpha)}}{g^{(\alpha)}} \left| \frac{\tau^{(\alpha)}}{g^{(\alpha)}} \right|^{\frac{1}{m}-1} \tag{9}$$

Here, γ_{0C} is the reference slip rate, $\tau^{(\alpha)} = \boldsymbol{T} : (\boldsymbol{s}^{(\alpha)} \otimes \boldsymbol{m}^{(\alpha)})_S$ is the resolved shear stress, $g^{(\alpha)}$ is the flow stress, and m is the strain-rate sensitivity. In this study, there is one slip system and the flow stress is constant.

3.3 Modeling of composite phase

We treat the lamellar structure consisting of the amorphous and crystalline phases in nano-order as a composite phase using the law of mixture (Argon, 2013). Generalized 3D laminate theory assumes that the deformation and stress of each phase are uniform, and the compatibility of these values is ignored in the interface between the amorphous and crystalline phases. When a constant strain condition is assumed for the composite phase, a high stress state is required for the crystalline phase that is a harder phase because the strain of the both phase must agree. In this study, we assume that the stress for the amorphous and crystalline phases is uniform, and the deformation rate tensor for the composite phase is expressed as the averaged stress of the amorphous and crystalline phases.

$$\boldsymbol{T} = \boldsymbol{T}_A = \boldsymbol{T}_C \tag{10}$$

$$\boldsymbol{D} = f_A \boldsymbol{D}_A + f_C \boldsymbol{D}_C \tag{11}$$

Here, $\boldsymbol{T}$ is the Cauchy stress for the composite phase, $\boldsymbol{D}$ is the deformation rate tensor for the composite phase, f_A is the volume fraction of the amorphous phase, and $f_C = 1 - f_A$ is the volume fraction of the crystalline phase. Equations (1), (8), (10), and (11) yield

ISSN NO: 9726-001X
Volume 10 Issue 03 2022

$$\overset{\nabla}{\boldsymbol{T}} = \boldsymbol{C}^e : \boldsymbol{D} - f_A \boldsymbol{C}^e : \boldsymbol{D}_A^p - f_C \boldsymbol{C}^e : \boldsymbol{D}_C^p, \tag{12}$$

$$\boldsymbol{C}^e = \boldsymbol{C}_A^e : (f_A \boldsymbol{C}_C^e + f_C \boldsymbol{C}_A^e / J)^{-1} : \boldsymbol{C}_C^e, \tag{13}$$

where $\overset{\nabla}{\boldsymbol{T}}$ is the corotational rate of Kirchhoff stress for the composite phase, J is the Jacobian, and $\boldsymbol{A}^{-1}$ means the inverse of the fourth-order tensor, i.e. $A_{ijmn} B_{mnkl} = \delta_{ik}\delta_{jl}$ ($\boldsymbol{B} = \boldsymbol{A}^{-1}$).

4. Simulation of PP

4.1 Numerical procedures

The present analysis employs a static explicit FEM. The deformation hysteresis is calculated using a linear incremental method at a constant edge-displacement speed. A PP specimen under plane strain is assumed in the current simulation. The initial aspect ratio of the specimen is $L/W = 3$ (Fig. 4(a)). An initial imperfection of 0.5% is applied to the edge of the specimen in the region of $L/3$ from the center of the specimen. Voronoi tessellation is adopted for generating spherulites, and Delaunay triangulation is adopted for meshing the FEM to express the inhomogeneity of the spherulite shape. There are 33,718 FEM elements, and the strain rate is 0.001s^{-1}. The boundary conditions for displacement $\boldsymbol{u}$ and load $\boldsymbol{F}$ are given by

$$\left.\begin{array}{ll} F_x = F_y = 0 & (\text{at } x = 0, W) \\ u_y = 0, F_x = 0 & (\text{at } y = 0) \\ u_y = U, F_x = 0 & (\text{at } y = L) \end{array}\right\}. \tag{14}$$

All elements are considered in the composite phase. In order to simulate a spherulite structure consisting of radially growing lamellae, we assume that the slip direction is perpendicular to the radial direction of the spherulite (Fig. 4(b)).

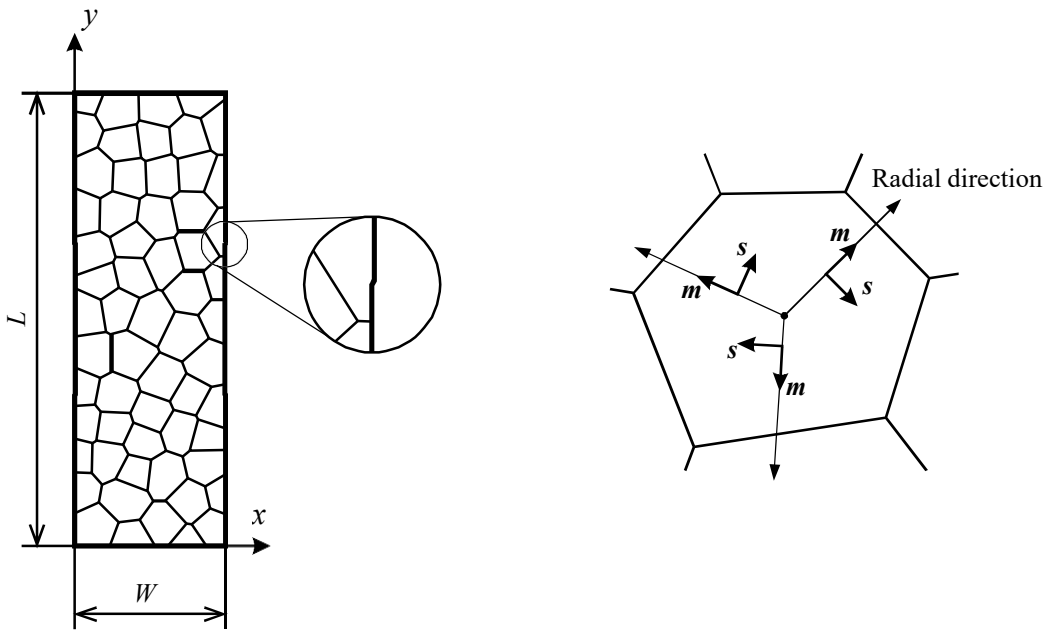

(a) Geometry of specimen (b) Crystal orientation in spherulite

Fig. 4 Geometry of the specimen, shape of spherulite in the specimen, and the initial crystal orientation of the crystalline phase. The black dot at the center of the spherulite coincides with a generator of the Voronoi diagram.

ISSN NO: 9726-001X
Volume 10 Issue 03 2022

The center of the spherulite coincides with the generators of the Voronoi diagram. The size of the spherulite is ignored because there is no size effect in the plasticity model used here.

The material constants and numerical parameters are the Young's modulus of the amorphous phase $E_A = 500$ MPa, the Poisson's ratio of the amorphous phase $\nu_A = 0.33$, the reference slip rate for the amorphous phase $\gamma_{0A} = 2\times10^{15}$ s^{-1}, the initial value of the athermal shear strength $s_0 = 40$ MPa, the saturated shear strength $s_{ss} = 27$ MPa, the hardening ratio $h = 200$, the absolute temperature $T = 296$ K, the numerical parameter $A = 580$, the pressure-dependent coefficient $\alpha = 0.08$, the number of molecular chains per unit volume $n = 4\times10^{27}$, the Boltzmann constant $k = 1.38\times10^{-29}$ MJ / K, the mean number of segments in a molecular chain $N = 4$, the Young's modulus of the crystalline phase $E_C = 1000$ MPa, the Poisson's ratio of the crystalline phase $\nu_C = 0.33$, the reference slip rate for the crystalline phase $\gamma_{0C} = 0.001$ s^{-1}, the flow stress $g^{(\alpha)} = 20$ MPa, and the strain rate sensitivity $m = 0.005$. A fluctuation of 10% due to heterogeneity of the material is assumed in the initial value of the athermal shear strength. The volume fraction of the crystalline phase f_C is 0.47, 0.56, or 0.60, obtained as described in Section 2.2. The material parameters on the amorphous phase is based on the literature (Tomita, 2000), whereas the values are changed proportionally so that the calculated yield stress and level stress approaches the experiment results. The material parameters on the crystalline phase is the usual values in crystal plasticity except the flow stress. The flow stress is decided from the comparison of numerical and experiment stress-strain curves.

4.2 Numerical results and discussion

Figure 5 plots the nominal stress versus nominal strain curves when the volume fractions of the crystalline phase f_C are 0.47, 0.56, and 0.60, which correspond to those of samples (i), (ii) and (iii), respectively. Table 2 presents the mechanical properties obtained by this simulation. The Young's modulus increases with increasing crystallinity. This tendency agrees well with the experiment results presented in Table 1. However, the yield stress for each crystallinity fraction is almost the same. The values of the level stress after yielding show the crosscurrents of the experiment result. The nominal stress for each crystallinity is equivalent after rehardening. The strain when the rehardening starts is less than that of the experiment results. One of the reason for the difference of the strain when the rehardening starts is the boundary condition of simulation. Since we assume the plane strain condition in this paper, a sectional area of the

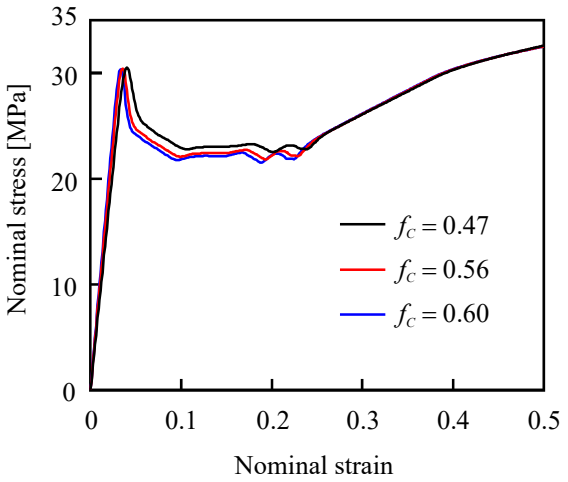

Fig. 5 Nominal stress versus nominal strain curves when the volume fractions of the crystalline phase are 0.47, 0.56, and 0.60.

Table 2 Mechanical properties determined by Fig. 5

f_C	Young's modulus [MPa]	Yield stress [MPa]
0.47	862.7	30.49
0.56	963.2	30.38
0.60	1016	30.34

ISSN NO: 9726-001X
Volume 10 Issue 03 2022

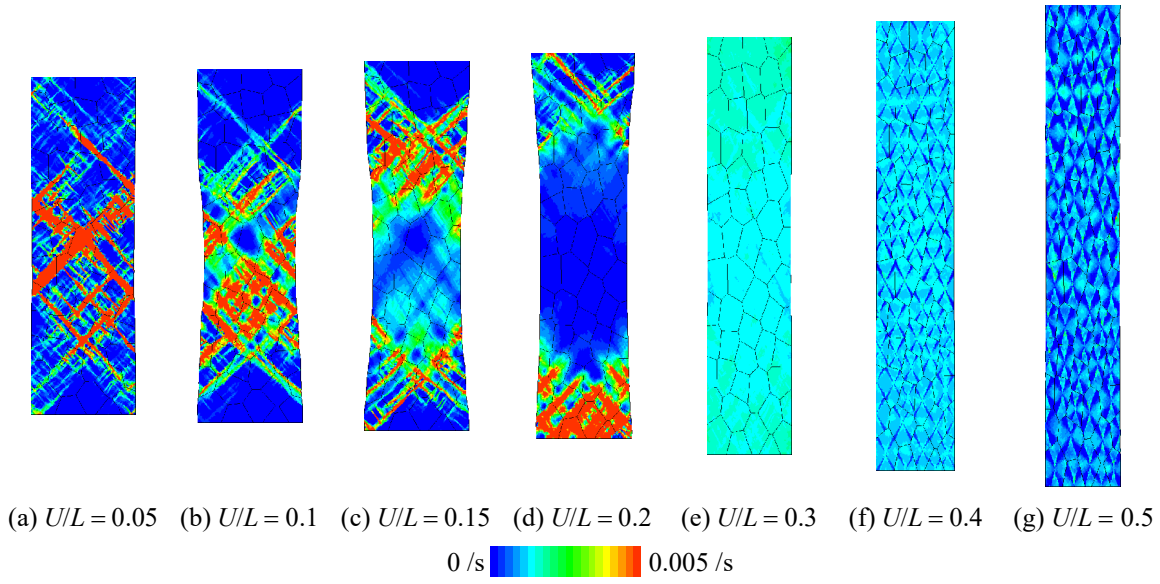

Fig. 6 Distributions of the equivalent plastic strain rate of the composite phase at each elongation percentage when the crystallinity is 0.47.

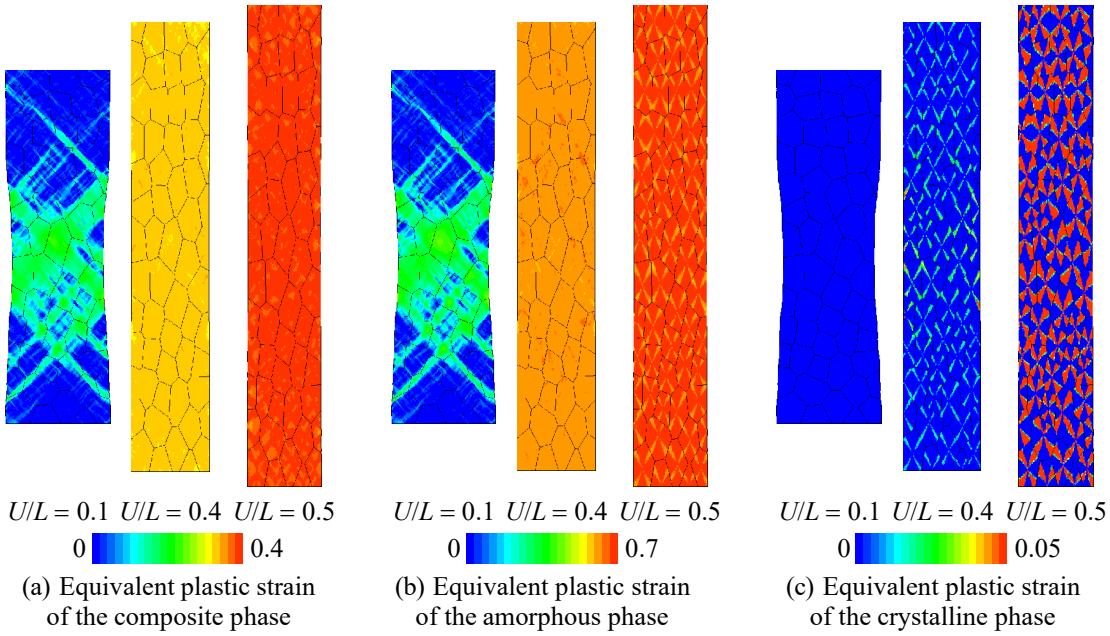

Fig. 7 Distributions of the equivalent plastic strain of the composite, amorphous, and crystalline phases at each elongation percentage when the crystallinity is 0.47.

specimen hardly changes. The ratio of the cross section after 50% elongation to the initial cross section is about 0.7, whereas the ratio obtained by the experiment is about 0.17 (f_C = 0.56). Moreover, the composite phase is harder than the pure amorphous phase because of the crystalline phase.

Figure 6 depicts the distribution of the equivalent plastic strain rate at each elongation percentage when $f_C = 0.47$. Distributions for the other crystallinity fractions are almost the same as Fig. 6. Micro-deformation bands are generated around the initial imperfections. Necking occurs after yielding, and the plastic deformation regions are propagated in the loading direction. When the propagation of necking covers an entire region of the specimen, rehardening begins, and the distribution of the equivalent plastic strain rate becomes almost uniform. After 40% elongation, a cross-shaped distribution is observed in all spherulites. Figure 7 depicts the distributions of equivalent plastic strain of the composite, amorphous, and crystalline phases. The distributions for the composite are similar to those for the amorphous phases when the elongation percentage is less than 40%. In contrast, the equivalent plastic strain for the crystalline phase is

ISSN NO: 9726-001X
Volume 10 Issue 03 2022

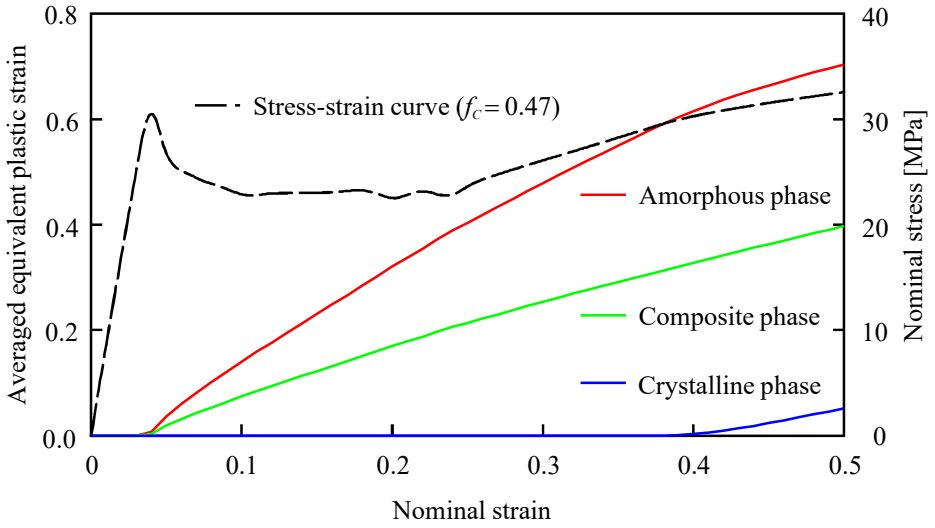

Fig. 8 Averaged equivalent plastic strain of the composite, amorphous and crystalline phases and the nominal stress versus nominal strain curves when the crystallinity is 0.47.

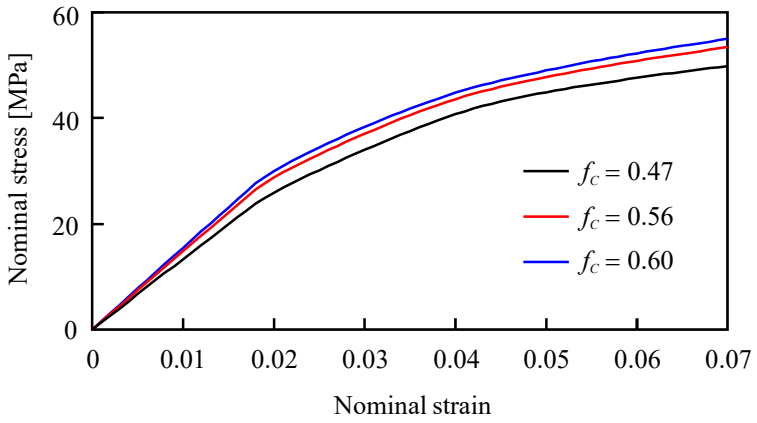

Fig. 9 Nominal stress versus nominal strain curves obtained by simulation using the constant strain condition for the law of mixture.

almost zero. When the elongation percentage reaches 40%, the slip system is activated in the region where the resolved shear stress, which depends on the slip direction and the normal direction of the slip plane, approaches the flow stress of the crystalline phase. In this simulation, the Schmid factor is maximum at an angle of 45 degree from the loading direction, causing the cross-shaped distribution depicted in Figs. 6 and 7. Figure 8 plots the equivalent plastic strain averaged in the specimen with the stress-strain curve when the crystallinity is 0.47. When plastic deformation occurs in the crystalline phase, the work-hardening ratio decreases. The same tendency is observed in the experiment curve, whereas the timing depends on the crystallinity (Fig. 3). We consider that the difference between the experiment and numerical curves is due to the size effect and a structure of the spherulite. The size of spherulite affects the material properties, because the crystallinity and the direction of lamellar structure actually depend on the distance from center of spherulite due to a growth process of spherulites. Moreover, the boundaries of the spherulites consist of the amorphous phase, and the volume fraction of the boundary is determined by the size of the spherulite. However, the crystallinity is uniform in a spherulite in order to simplify the modeling of spherulite in this paper investigating the effect of mesoscopic crystallinity. Figure 9 plots the nominal stress versus nominal strain curves obtained by simulation using the constant strain condition for the law of mixture. Figure 9 predicts the crystallinity dependency on the yield stress and the elasticity behavior, whereas the softening after yielding does not occur in a stress-strain curve, and no necking appears. The direction of lamellar structure affects the law of mixture for the composite phase. There is quite a possibility that combination of the constant strain and the constant stress conditions, which is based on the direction of lamellar structure, reproduces the dependency of the stress-strain curve on crystallinity and the propagation of necking, simultaneously.

5. Conclusions

With the spherulite structure including amorphous and crystalline phases, we conduct a polymer plasticity simulation. Explicit experimental data on spherulite crystallinity is fed into a computer model. Furthermore, we contrast the experimental findings from tensile testing with the computational results. We look at the PP material qualities and how the spherulite structure affects them. The following are our findings.
A combination of the constitutive equations for the amorphous and crystalline phases, using the law of mixing, expresses the composite phase, which is composed of the two phases.
(2) Under the constant stress condition for the law of mixing, the yield stress in the simulation remains independent of crystallinity, despite the fact that Young's modulus is crystallinity dependent.

(3) A drop in the work-hardening ratio and the appearance of a cross-shaped distribution of strain are the results of plastic deformation in the crystalline phase.

Acknowledgments

The author would like to thank Professor T. Okabe for valuable discussions throughout this work. This study is financially supported by a Grant-in-Aid for Exploratory Research through MEXT, Japan (contract No. 25630003), and the authors deeply appreciate this support.

References

Aboulfaraj, M., Ulrich, B., Dahoun, A. and Sell, C. G., Spherulitic Morphology of Isotactic Polypropylene Investigated by Scanning Electron Microscopy, Polymer, Vol. 34, No. 23 (1993), pp. 4817-4825.

Argon, A. S., The Physics of Deformation and Fracture of Polymers (2013), p. 315, Cambridge University Press.

Arruda, E. M. and Boyce, M. C., Evolution of Plastic Anisotropy in Amorphous Polymers during Finite Straining, International Journal of Plasticity, Vol. 9, No. 6 (1993a), pp. 697-720

Arruda, E. M. and Boyce, M. C., A Three-dimensional Constitutive Model for the Large Stretch Behavior of Rubber Elastic Materials, Journal of the Mechanics and Physics of Solids, Vol. 41, No. 2 (1993b), pp. 389-412.

Bowden, P. B. and Young, R. J., Deformation Mechanisms in Crystalline Polymers, Journal of Materials Science, Vol. 9 (1974), pp. 2034-2051.

Boyce, M. C., Parks, D. M. and Argon, A. S., Large Inelastic Deformation of Glassy Polymers Part I: Rate Dependent Constitutive Model, Mechanics of Materials, Vol. 7 (1988), pp. 15-33.

Boyce, M. C., Parks, D. M. and Argon, A. S., Plastic Flow in Oriented Glassy Polymers, International Journal of Plasticity, Vol. 5, No. 6 (1989), pp. 593-615.

Kubo, M., Katagiri, M. and Hori, Y., FEM Analysis of Stress Distribution in the Spherulite, Transactions of the Japan Society of Mechanical Engineers, Series A, Vol. 52, No. 474 (1986), pp. 557-560 (in Japanese).

Nada, H. and Shizawa, K., Molecular Chain Plasticity Model Like Crystal Plasticity Theory Using Probabilistic Response Law of Inelasticity Based on Change of Local Free Volume for Glassy Polymer, Transactions of the Japan Society of Mechanical Engineers, Series A, Vol. 74, No. 737 (2008a), pp. 97-104 (in Japanese).

Nada, H. and Shizawa, K., Large Deformation Analysis for Glassy Polymer Based on Molecular Chain Plasticity Model Like Crystal Plasticity Theory Considering Change of Local Free Volume, Transactions of the Japan Society of Mechanical Engineers, Series A, Vol. 74, No. 737 (2008b), pp. 105-114 (in Japanese).

Pan, J. and Rice, J. R., Rate Sensitivity of Plastic Flow and Implications for Yield-Surface Vertices, International Journal of Solids and Structures, Vol. 19, No. 11 (1983), pp. 973-987.

Parks, D. M. and Ahzi, S., Micromechanical Modeling of Large Plastic Deformation and Texture Evolution in Semi-crystalline Polymers, Journal of the Mechanics and Physics of Solids, Vol. 41, No. 10 (1993), pp. 1651-1687.

Peirce, D., Asaro, R. J. and Needleman, A., Material Rate Dependence and Localized Deformation in Crystalline Solids, Acta Metallurgica, Vol. 31, No. 12 (1983), pp. 1951-1976.

Tomita, Y. and Tanaka, S., Prediction of Deformation Behavior of Glassy Polymers Based on Molecular Chain Network

Model, International Journal of Solids and Structures, Vol. 32, No. 23 (1995), pp. 3423-3434.

Tomita, Y., Constitutive Modeling of Deformation Behavior of Glassy Polymers and Applications, International Journal of Mechanical Sciences, Vol. 42, No. 8 (2000), pp. 1455-1469.

Uchida, M. and Tada, N., Micro-, Meso- to Macroscopic Modeling of Deformation Behavior of Semi-crystalline Polymer, International Journal of Plasticity, Vol. 49 (2013), pp. 164-184.

Wu, P. D. and van der Giessen, E., On Neck Propagation in Amorphous Glassy Polymers under Plane Strain Tension, International Journal of Plasticity, Vol. 11, No. 3 (1995), pp. 211-235.